AVALANCHES ON MT. FUJI, JAPAN: SEISMIC DETECTION AND TRACKING COMBINED WITH NUMERICAL SIMULATIONS

Pérez-Guillén Cristina[1,2,*], Tsunematsu Kae[3,4], Nishimura Kouichi[1], Issler Dieter[5]

[1]*Graduate School of Environmental Studies, Nagoya University, Japan*
[2]Now at: *RISKNAT Avalanche Research Group, University of Barcelona, Spain*
[3]*Mount Fuji Research Institute, Yamanashi Prefectural Government, Japan*
[4]Now at: *Dept. of Earth and Environmental Sciences, Yamagata University, Yamagata, Japan*
[5]*Norwegian Geotechnical Institute, Oslo, Norway*

ABSTRACT: Avalanches from Mt. Fuji may attain run-out distances of up to 3 km and represent a major natural hazard. These avalanches exhibit different flow types from typical dry-snow avalanches in winter to slush flows triggered by heavy rain in spring. For monitoring the volcanic activity of Mt. Fuji, a dense permanent seismic network is installed around the volcano. The seismic recordings are used here to identify avalanche events and locate them in time and space. Applying the amplitude source location (ASL) method for the first time to avalanches, several avalanche events have been seismically identified in each of three analyzed avalanche periods in the winters of 2014, 2016 and 2018. The largest avalanches (size class 4–5) are detected by the seismic sensors at distances up to 15 km, medium-size events within a radius of 9 km. The joint analysis of several seismic stations allowed localizing and tracking these avalanches so that the run-out distances and velocities could be estimated. The accuracy of the seismic tracking was analyzed by simulating the avalanches with the dynamical model Titan2D, using aerial photos and meteorological records to estimate the release areas and volumes.

Keywords: Snow avalanches, seismic detection, avalanche location, numerical simulations

1. INTRODUCTION

Dedicated seismic monitoring systems, deployed at an endangered site, are a powerful tool for detecting different types of natural hazards. Snow avalanches reveal themselves as non-emergent, long-lasting (> 10s), high-frequency (1–100 Hz) signals in seismic recordings. These specific seismic patterns can be used for avalanche monitoring (Suriñach et al., 2001), automatic avalanche identification (Hammer et al., 2017; Heck et al., 2018), flow speed determination (Vilajosana et al., 2007; Lacroix et al., 2012), and flow type and size characterization (Pérez-Guillén et al., 2016). So far, seismic sensors for earthquake or volcano monitoring have been rarely used for locating avalanches because of methodical limitations. For instance, traditional earthquake localization procedures are not suitable for avalanches as they are based on the arrival times of different seismic phases, which are not usually distinguishable in the avalanche recordings.

The usual method for locating multiple moving seismic sources is based on beam-forming techniques that exploit the cross-correlation of signals from several seismic sensors deployed as a seismic array (Almendros et al., 1999). Using this methodology, Lacroix et al. (2012), successfully localized eighty snow avalanches in the French Alps. However, this method requires installing the seismic sensors in a specific configuration where source–receiver distances are at least four times larger than the aperture of the seismic array (Almendros et al., 1999). An alternative method to locate seismic sources is the amplitude source location (ASL) method that is based on the spatial distribution of the seismic amplitudes. This method is able to localize avalanches with a more open distribution of sensors and has been used previously to locate different types of mass movements such as lahars (Kumagai et al., 2010) and debris flows (Ogiso and Yomogida, 2015; Walter et al., 2017).

In this study, we applied the ASL method for the first time to locate snow avalanches and slush flows on the slopes of Mt. Fuji. At 3776 m a.s.l., it is the highest mountain of Japan and towers almost 2000 m above all mountains within a range of 50 km. It receives large amounts of snow every winter. Snow avalanches at Mt. Fuji release often and can reach large dimensions with run-out distances up to 3 km; they regularly destroy parts of the forest and sometimes damage infrastructures.

Mt. Fuji being a stratovolcano in proximity of the Tokyo metropolitan area, there is a permanent seismic network installed around the volcano to monitor its seismicity (Fig. 1). The small distance between the sensors and the volcano flank (< 10 km) allowed

*Corresponding author address:
Graduate School of Environmental Studies, Nagoya University, Japan
email: cris.perez.guillen@gmail.com

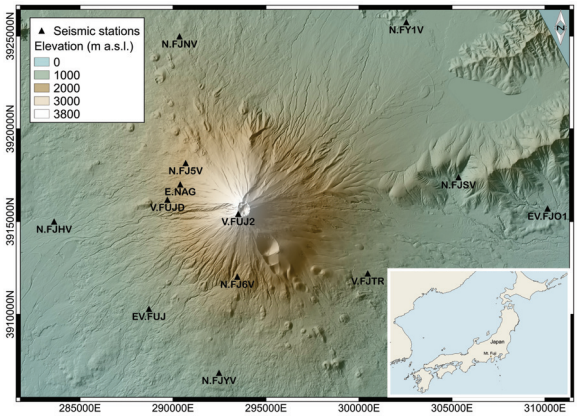

Figure 1: General map of Japan with the location of Mt.Fuji (inset) and topographic map of the Mt. Fuji region with the location of the 13 seismic stations used for this study. Stations are labeled according to the institutions that operate them: N.F* (National Research Institute for Earth Science and Disaster Resilience, NIED), EV.* (University of Tokyo), V.* (Japan Meteorological Agency, JMA) and E.NAG (Nagoya University and Mount Fuji Research Institute). E.NAG is a temporary seismic station installed during the winter seasons 2016 and 2017 to monitor avalanches released in an active path on the WNW flank of Mt. Fuji.

us to detect, characterize and localize numerous avalanche events on Mt. Fuji. We then used numerical simulations with dynamical avalanche models such as Titan2D to reconstruct the avalanche trajectories and in this way to assess the precision of the ASL method. We also determined the minimum number of stations required to locate avalanches in this region. Meteorological data and images of the flow deposits were used as complementary data for assessing avalanche risk on the slopes of Mt. Fuji. To date, we have identified eight avalanches and slush flows triggered in three avalanche periods in the winters of 2014, 2016 and 2018. For each of these periods, more than one avalanche event has been detected seismically in short time windows of a few hours during heavy precipitation episodes. Due to space limitations, we focus on a single avalanche event of 2014 in the following analysis.

2. METHODS AND EVENTS

2.1. The avalanche event of 2014

At this stage of development, we used information about observed avalanche deposits, aerial photos and weather data to constrain the time window within which to search manually for avalanche signals in the seismic data from the local seismic network of Mt. Fuji (Fig. 1). This network consists of short-period (1 Hz), three-component seismometers with a sampling frequency of 100 Hz. Other seismic sources could be discarded by comparing the candidate events with a regional seismic catalog provided by NIED.

A spontaneously released avalanche descended the west-northwestern (WNW) flank of Mt. Fuji on 2014-03-13 (here referred to as avalanche #1). An aerial photograph taken after the event shows the deposits of a large avalanche (size 4–5) that impacted the road, destroying part of the nearby forest (Fig. 2.a). This avalanche was first seismically detected at 18:14:43 by the V.FUJ2 station (Fig. 2.b), which is located at the summit of the volcano. At this time, the records from the automatic weather station at 2020 m a.s.l. (location of E.NAG in Fig. 1) reported a temperature of 5 °C and a cumulative precipitation of 140 mm in the 12 hours before the avalanche release; the wind speed ranged from 4 to 16 m s^{-1} during the previous 24 hours, blowing mainly from SE and S directions.

The normalized vertical seismograms recorded at each location are shown in Fig. 2.b, ordered according to increasing distance from the avalanche. V.FUJD station was closest (∼1 km from the run-out area) and EV.FJO1 farthest at a distance of ∼20 km. In general, maximum amplitudes decrease as a function of distance to the source. However, some stations (V.* and EV.*) show great amplifications due to local site effects. This avalanche was detected by 11 seismic stations at a maximum distance of 15 km. The signals show the typical spindle shape of avalanches (Pérez-Guillén et al., 2016): a gradual increase of the amplitudes until the arrival of maximum amplitudes at 18:15:35 (Fig. 2.b). The triangular increase observed in the spectrogram of V.FUJD (Fig. 2.b) shows that the flow is approaching the sensor. The time interval of the maximum amplitudes is thus correlated with the arrival of the flow in the run-out area (path #1 of Fig. 2.b), followed by a decrease of the amplitudes that is characteristic of avalanche deposition (from 18:15:45 to 18:16:10). Another long wave packet, from 18:16:10 to 18:23:30 of Fig. 2.b, is detected by the stations closest to the run-out area (V.FUJD and N.FJ5V stations). The spectrogram generated by this second surge is characterized by a temporal increase of the high-frequency energy content (up to 20 Hz; Fig. 2.b) likely generated by a part of the avalanche that is slowly moving downwards, following a gully that approaches the location of V.FUJD (path #2 of Fig. 2.a).

2.2. Amplitude source location

The ASL method compares the recorded amplitudes at several sensor locations $\mathbf{x}_j$ with the expected amplitudes that are derived from fundamental properties of wave propagation, namely (i) geometrical attenuation due to spreading, (ii) attenuation due to absorption during propagation, and (iii) local site effects. The method assumes isotropic radiation of S waves at high frequency (see Kuma-

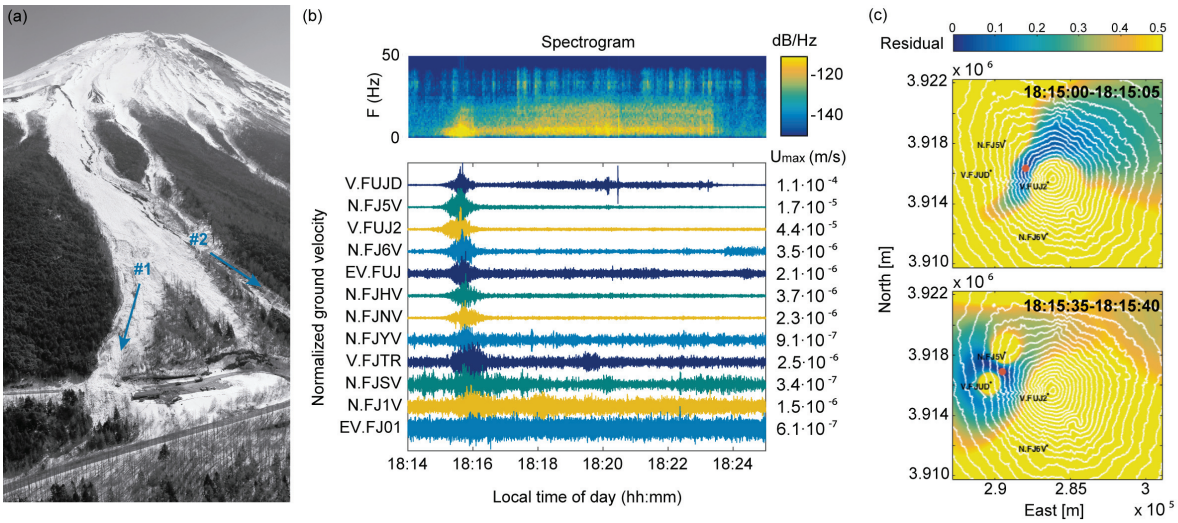

Figure 2: (a) Aerial photo of the large avalanche #1 released on 13 March, 2014 (source: Asahi Shimbun Digital (www.asahi.com). The main flow impacted on the road (path #1) and a secondary surge continued flowing downwards following path #2. (b) Spectrogram (computed at the V.FUJD station) and vertical seismograms generated by the avalanche #1 at the different stations, which are ordered according to the distance from the run-out area. Each trace is normalized by its maximum amplitude, U_{max}. (c) Spatial distribution of the residuals estimated for the avalanche #1 in two different time intervals: the beginning of the avalanche signal (upper panel) and the maximum amplitudes recorded (lower panel).

gai et al. (2010) for a detailed description of the method). The source location, $\mathbf{x}$, is estimated by minimizing the residual,

$$R = \frac{\sum_{j=1}^{N} \left[u_j^o(t_s + r_j/\beta) - A_0 \frac{e^{-Br_j}}{r_j} \right]^2}{\sum_{j=1}^{N} \left[u_j^o(t_s + r_j/\beta) \right]^2} \qquad (1)$$

over all possible source locations. N is the total number of stations, t_s is the signal emission time, $r_j \equiv \|\mathbf{x} - \mathbf{x}_j\|$ is the distance between the source and the jth station, β is the seismic wave velocity, and u_j^o is the observed amplitude at the jth station. The second term of the numerator of Eq. 1 is the decay relationship of the seismic amplitudes due to the attenuation of body waves with distance, with A_0 the signal amplitude at the source. The factor $1/r_j$ accounts for purely geometric attenuation, while $\exp(-Br_j)$ represents absorption with mean attenuation coefficient $B = \pi f/(Q\beta)$. The latter depends on the quality factor Q, the seismic velocity β in the medium and the frequency f of the waves.

The raw amplitudes at each station were corrected with site amplification factors that account for local focusing effects on seismic waves due to the topography and soil stratification. These factors can be obtained by analyzing signals from regional earthquakes. In Eq. (1), the observed amplitudes $u_j^o(t)$ already contain the respective site amplification factors.

Equation (1) is minimized by sampling $\mathbf{x}$ at the nodes of a regular grid. In the present study, the source–sensor distances r_j were calculated using a digital elevation model (DEM) with 10 m resolution. The dimension of the grid was about 14 km (East) by 12.5 km (North), which includes all the potential avalanche paths of Mt. Fuji. The observed vertical components of avalanche signals were filtered using a band-pass filter between 4 and 8 Hz. We estimated the mean amplitudes of the envelope using a 5 s wide sliding window, shifting it at 1 s increments. At each location, the amplitudes are corrected by the site amplification factors and the emission-time window is shifted according to the S-wave travel times. We used a mean S-wave velocity of $\beta = 1400\,\mathrm{m\,s^{-1}}$, typical of volcanic surface material (Ogiso and Yomogida, 2015). A quality factor $Q = 125$ was adopted after testing a range of Q values.

2.3. Avalanche tracking

For locating an avalanche, we use all stations that have a sufficient signal-to-noise ratio over a time interval of at least 1 min. We discard the initial and final parts of the avalanche signal because these are detected by too few sensors. Figure 2.c displays the residual distributions estimated in two different time windows corresponding to (i) the beginning of the avalanche signal (18:15:00–18:15:05) and the maximum energy recorded by V.FUJD station (18:15:35–18:15:40). A region of small residuals is observed at higher altitudes on the NW flank of Mt. Fuji with the minimum location at 2790 m a.s.l. on the WNW side (Fig. 2.c, upper panel). The second residual distribution shows a region of small residuals located between two stations (N.FJ5V and V.FUJD) on the WNW flank with the minimum at 2060 m a.s.l. that is located in the avalanche run-out area (Fig. 2.c, lower

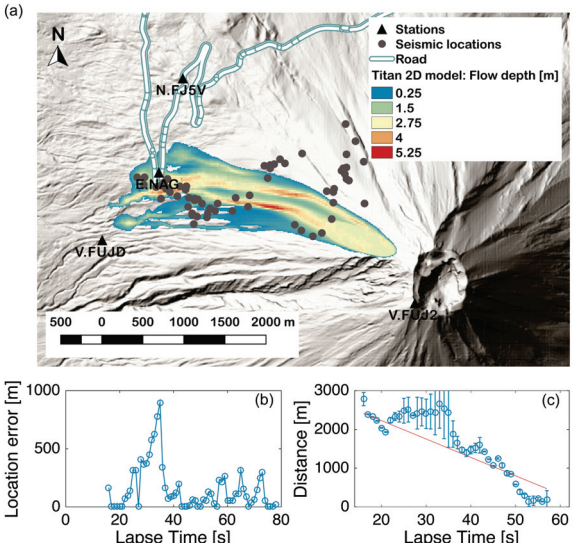

Figure 3: (a) Simulated flow depth with the dynamical model Titan2D of the avalanche #1 and estimated avalanche locations (grey points) from the seismic analysis. (b) Location error estimated as a function of lapse time from the simulation start time. (c) Distance of the seismic location from seismometer E.NAG as a function of lapse time. The line shows the linear regression fit.

panel). A map of the locations of the minimum residuals is plotted in Fig. 3.a. In general, the minimum residual distributions are located in the WNW path of Mt. Fuji, in accord with the field observations. Initial points are located at a maximum elevation of 3200 m a.s.l. and final locations at about 2000 m a.s.l. The seismic locations extend over a distance of about 2.5 km.

3. PRECISION OF THE LOCATION METHOD

3.1. Numerical simulations and seismic locations

We conducted numerical simulations of the avalanche flows with the numerical model Titan2D that is designed for simulating mass flows based on the depth-averaged balance equations for mass and momentum of an incompressible continuum, a "shallow-water" granular flow (Patra et al., 2005). From considerations of topography and wind conditions, the most likely release area is centered at 3300 m a.s.l. on the WNW flank with mean slopes between 35° and 45°. The precipitation and wind speeds measured at lower altitude suggest a fracture depth of ~2.5 m. We determined the approximate bounds of the run-out area from the aerial photo and the recorded damage (Fig. 2.a). With this, simulations reproduce the deposition pattern satisfactorily if the Coulomb friction coefficient is set to $\mu_1 = \tan 20°$ above 2500 m a.s.l. and $\mu_2 = \tan 25°$ below 2500 m a.s.l., thus accounting for differences in snow temperature. The flow depth simulated for this avalanche is shown in Fig. 3.a. Note that the avalanche has several branches.

The numerical simulation provides a reference for assessing the precision of the ASL method. We compared the seismic location at each time interval with the evolution of the simulated avalanche flow. Seismic locations could be determined only about 12 s after the avalanche signal first emerges from the noise at station V.FUJ2 at the summit of the volcano. We also assumed an additional delay of a few seconds because the first movements of the avalanche are unlikely to generate enough seismic energy to be detected at a distance of ~1 km. This second time delay was estimated by minimizing the mean error in the locations.

We define the location error as the minimum distance between the avalanche flow and the punctual seismic location. We set this value to zero if the seismic location is within the avalanche flow. Figure 3.b shows the location errors as a function of the lapse time from the start of the simulation. The mean location error is 154 m and 25% of the locations are within the avalanche flow. Figure 3.a shows an interval of erroneous migrations of the locations to the NW direction at 28–36 s with location errors over 400 m (Fig. 3.b). Ogiso and Yomogida (2015) also observed migrations of the locations in a wrong direction, probably caused by an inadequate distribution of stations in that phase. The lack of stations close to the release area may explain the observed migrations in our case (Fig. 3.a). The residual distribution in the first part of the avalanche signal also shows that the region of small residuals extended in NW direction (Fig. 2.c, upper panel). Figure 3.c shows the distance calculated from the seismic locations to the sensor E.NAG in the run-out area (Fig. 3.a) as a function of time. From the linear regression of distance versus time, we estimate the average velocity at $47.4 \pm 1.5\,\mathrm{m\,s^{-1}}$.

3.2. How many stations are needed?

From our study, one can obtain an indication of the required density of a seismic network for detecting and localizing avalanche activity. The largest avalanches (size class 4–5) are detected by the seismic sensors at maximum distances of about 15 km (e.g., avalanche #1 of Figure 2), medium-size events within a radius of 9 km. To test the number of sensors required, we calculated the location errors using a variable number of stations to locate the avalanche signal (Fig. 4). The minimum number of sensors required to locate avalanche #1 is three. The location errors in the first part of the avalanche motion ($t < 30$ s), however, are very high with values up to 9 km. A minimum number of six sensors, within a radius of 1–6 km, is required to obtain locations with satisfactory precision (mean location error below 200 m).

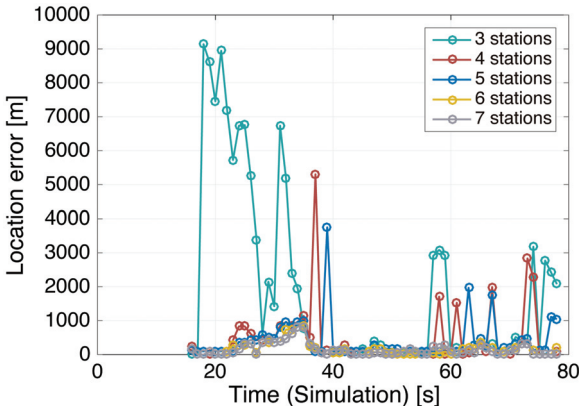

Figure 4: Comparison of the time evolution of location errors using from three to seven sensors.

4. CONCLUSIONS

The ASL method is/has proven a useful technique for locating the position of the main avalanche flows in an extended area where a seismic network with an average distance between the sensors of up to 6 km is available. A minimum of three sensors is required to locate the avalanche, but the precision is then quite poor. Higher-precision locations are obtained using six or more sensors distributed in a pattern that facilitates triangulation. Our results show that it is feasible to determine in which path an avalanche released, to track the avalanche flow with reasonable precision and to infer additional parameters such as the approximate run-out distance and the average velocity of the flow. This is very valuable information for assessing avalanche risk on Mt. Fuji as seismic records are the only available information on snow avalanche events in most cases. More generally, our study suggests that using ASL one may expect to detect and track avalanches in size class 4–5 with ten sensors per 100 km^2; for size class 3, at least three sensors per 30 km^2 would be required.

An important task in the near future will be to develop highly effective and efficient algorithms for automatically detecting and tracking avalanche events in the seismic data in near-real-time. Judging from work done in the context of beam-forming methods (Lacroix et al., 2012), we expect this goal to be achievable in the near future. More research is also needed to improve the results in situations with multiple simultaneous, but spatially well separated strong sources of seismic energy. This can be the case, e.g., when an avalanche is split into two branches, when secondary releases occur or when the avalanche continues to impact on a fixed obstacle while the front moves ahead. Once these problems are solved, this inexpensive method for wide-area monitoring of avalanche activity should find application in many regions.

ACKNOWLEDGEMENTS

The first author was supported by a short-term post-doctoral fellowship (FY2017–2018) from the Japan Society for the Promotion of Science (JSPS). We thank Prof. Shinichi Sakai at the Earthquake Research Institute of Tokyo University and Dr. Hideki Ueda and Dr. Taishi Yamada at the National Research Institute for Earth Science and Disaster Resilience, and the Japan Meteorological Agency for providing the seismic data and related information. We thank the Mt. Fuji Toll Road Administrative Office, Yamanashi Prefecture for providing the meteorological data. We are also grateful to Dr. Ryo Honda and Dr. Mitsuhiro Yoshimoto of the Mount Fuji Research Institute, and Dr. Shinichiro Horikawa of the Nagoya University for their support.

REFERENCES

Almendros, J., Ibáñez, J. M., Alguacil, G. and Del Pezzo, E. (1999). Array analysis using circular-wave-front geometry: an application to locate the nearby seismo-volcanic source. *Geophysical Journal International*, 136(1), 159–170.

Hammer, C., Fäh, D. and Ohrnberger, M. (2017). Automatic detection of wet-snow avalanche seismic signals. *Natural Hazards*, 864(2):601–618.

Heck, M., Hammer, C., Van Herwijnen, A., Schweizer, J., Fäh, D. (2018). Automatic detection of snow avalanches in continuous seismic data using hidden Markov models. *Natural Hazards and Earth System Sciences*, 18(1):383–396.

Kumagai, H., Nakano, M., Maeda, T., Yepes, H., Palacios, P., Ruiz, M., Arrais, S., Vaca, M., Molina, I. and Yamashima, T. (2010). Broadband seismic monitoring of active volcanoes using deterministic and stochastic approaches. *Journal of Geophysical Research: Solid Earth*, 115(8):1–21.

Lacroix, P., Grasso, J. R., Roulle, J., Giraud, G., Goetz, D., Morin, S. and Helmstetter, A. (2012). Monitoring of snow avalanches using a seismic array: Location, speed estimation, and relationships to meteorological variables. *Journal of Geophysical Research: Earth Surface*, 117(1):1–15.

Ogiso, M. and Yomogida, K. (2015). Estimation of locations and migration of debris flows on Izu-Oshima Island, Japan, on 16 October 2013 by the distribution of high frequency seismic amplitudes. *Journal of Volcanology and Geothermal Research*, 298:15–26.

Patra, A. K., Bauer, A. C., Nichita, C.C., Pitman, E. B., Sheridan, M. F., Bursik, M., Rupp, B., Webber, A., Stinton, A. J., Namikawa, L. M. and Renschler, C. S. (2005). Parallel adaptive numerical simulation of dry avalanches over natural terrain. *Journal of Volcanology and Geothermal Research*, 139(1-2):1–21.

Pérez-Guillén, C., Sovilla, B.,Suriñach, E., Tapia, M. and Köhler, A. (2016). Deducing avalanche size and flow regimes from seismic measurements. *Cold Regions Science and Technology*, 121:25–41.

Suriñach, E., Furdada, G., Sabot, F., Biescas, B. and Vilaplana, J.M. (2001). On the characterization of seismic signals generated by snow avalanches for monitoring purposes. *Annals of Glaciology*, 32(1):268–274.

Vilajosana, I., Khazaradze, G., Suriñach, E., Lied, E. and Kristensen, K. (2007). Snow avalanche speed determination using seismic methods. *Cold Regions Science and Technology*, 49(1):2–10.

Walter, F., Burtin, A., McArdell, B., Hovius, N., Weder, B. and Turowski, J. (2017). Testing seismic amplitude source location for fast debris-flow detection at Illgraben, Switzerland. Natural Hazards and Earth System Sciences, 6:939–955.